Chapter 7

Studies on Structural and Mechanical Characterization of CoO and CeO_2 Doped Fe-Al_2O_3 Metal Matrix Nanocomposites

Chapter 7
Studies on Structural and Mechanical Characterization of CoO and CeO_2 Doped Fe-Al_2O_3 Metal Matrix Nanocomposites

The present chapter focuses on the effect of addition of cobalt oxide and cerium oxide to Fe-Al_2O_3 metal matrix nanocomposites. Various properties investigated include XRD, SEM, density, hardness and wear.

7.1 CoO Doped Fe-Al_2O_3 Metal Matrix Nanocomposites

Fe-Al_2O_3 Metal Matrix Nanocomposite specimen doped with 0.5 and 1.0% CoO were synthesized by powder metallurgy technique. Powders of electrolytic grade iron metal (99.5% purity and particle size 250-300 mesh (49-58 μm)) and active aluminum oxide (particle size 70-230 mesh (63-210 μm)) and cobalt oxide (99% purity) were used as starting materials. Composition of the composite was 90% Fe and 10% Al_2O_3 by weight. Additional 0.5 and 1.0% by weight of the cobalt oxide was used as a dopant in this composite system. Appropriate mixtures of Fe, Al_2O_3, CoO and binder were milled using zirconia balls as the grinding and mixing media with powder to ball ratio of 1:2. The composition was dry ball milled for 2 hours. For first 30 minutes Al_2O_3 and CoO was ball milled. For the next 30 minutes Fe was added to the above mixture and the whole mixture was again ball milled. Finally dextrin was added to the whole composition and was ball milled for 1 more hour. The mixed composition was compacted in a die of 13 mm diameter under a load of 7 tons. Sintering of the green compacts was carried out in an argon atmosphere at 1100°C for 1h. Specimens of pure iron and with 0.5 wt% CoO without Al_2O_3 (i.e. Pure Fe and 0.5 wt% CoO) were also prepared to compare the characteristics of the composite specimens and iron specimens. After sintering, the compacts were machined. It was found that the machinability of the specimens was better than the un-doped specimens. Initially the dimensions of the specimen was 20 mm height and 13 mm diameter, after the sintering process and after machining the dimensions of the specimens were 18 mm

height and 12 mm diameter respectively. A nomenclature e.g. 10AFe0.5Co1100(1) is given to each specimen. Here A denotes aluminum oxide, Fe denotes iron, 0.5Co denotes the percentage of cobalt oxide, 1100 denotes the sintering temperature, 1 denotes time of sintering.

7.1.1 X-ray Diffraction

XRD patterns of (a) 10AFe0.5Co1100(1), (b) 10AFe1.0Co1100(1) and (c) Pure Fe+0.5% Co are shown in Fig. 7.1. From the XRD - JCPDS matching, it was found that Fe, Al_2O_3 and CoO phases are present in the composite specimens. This shows that there no reaction has taken place among Fe, Al_2O_3 and CoO which are present in the composite specimen. Thus, in this Fe - Al_2O_3 composite system sintering is non-reactive sintering and Fe, Al_2O_3 and CoO are present as separate phases.

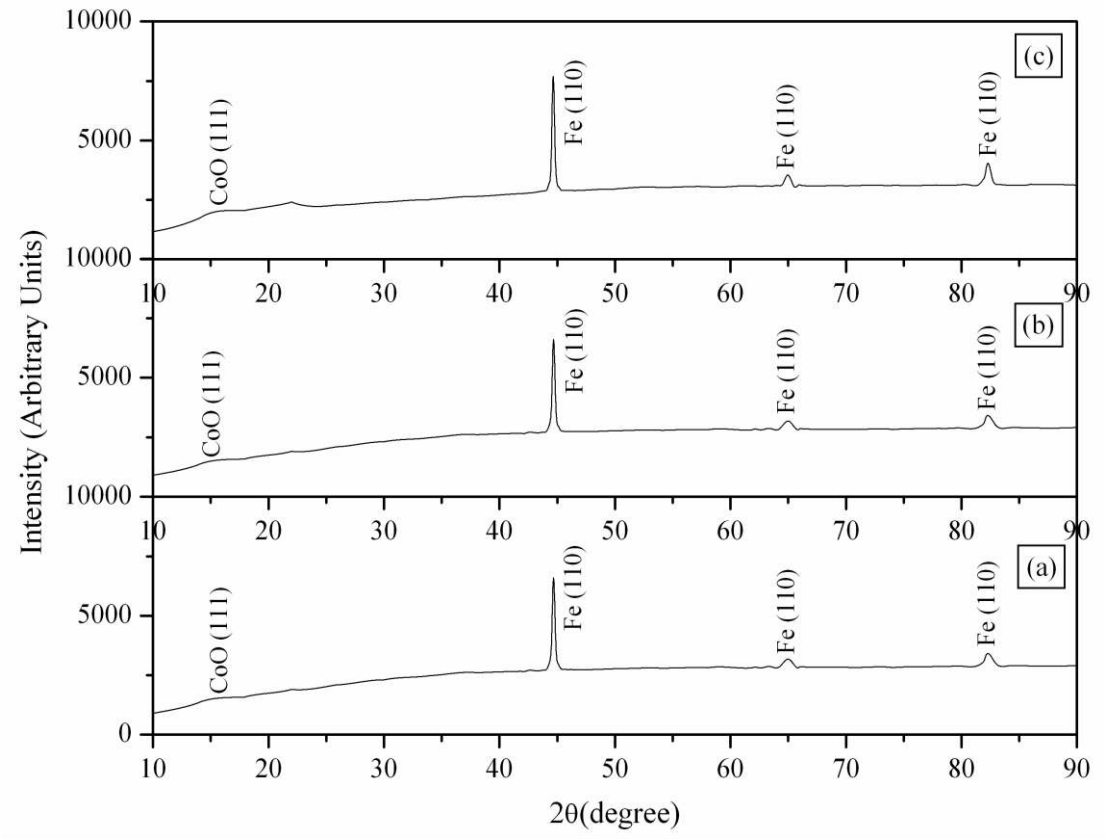

Fig. 7.1 XRD plots of (a) 10AFe0.5Co1100(1) (b) 10AFe1.0Co1100(1) and (c) Pure Fe+0.5%CoO

7.1.2 Scanning Electron Microscopy

SEM micrograph for the polished and etched specimen 10AFe0.5Co1100(1) is shown in Fig. 7.2. Microstructure at 1000X magnification (Fig. 7.2 (a)) reveals the formation of dense Fe-Al_2O_3-CoO metal matrix composite with some porosity in and around iron grains. In Fig. 7.2 (b) the larger black grains are of iron, white are of alumina whereas the rest of the grains are of cobalt oxide which is present on the periphery of the grains of iron itself.

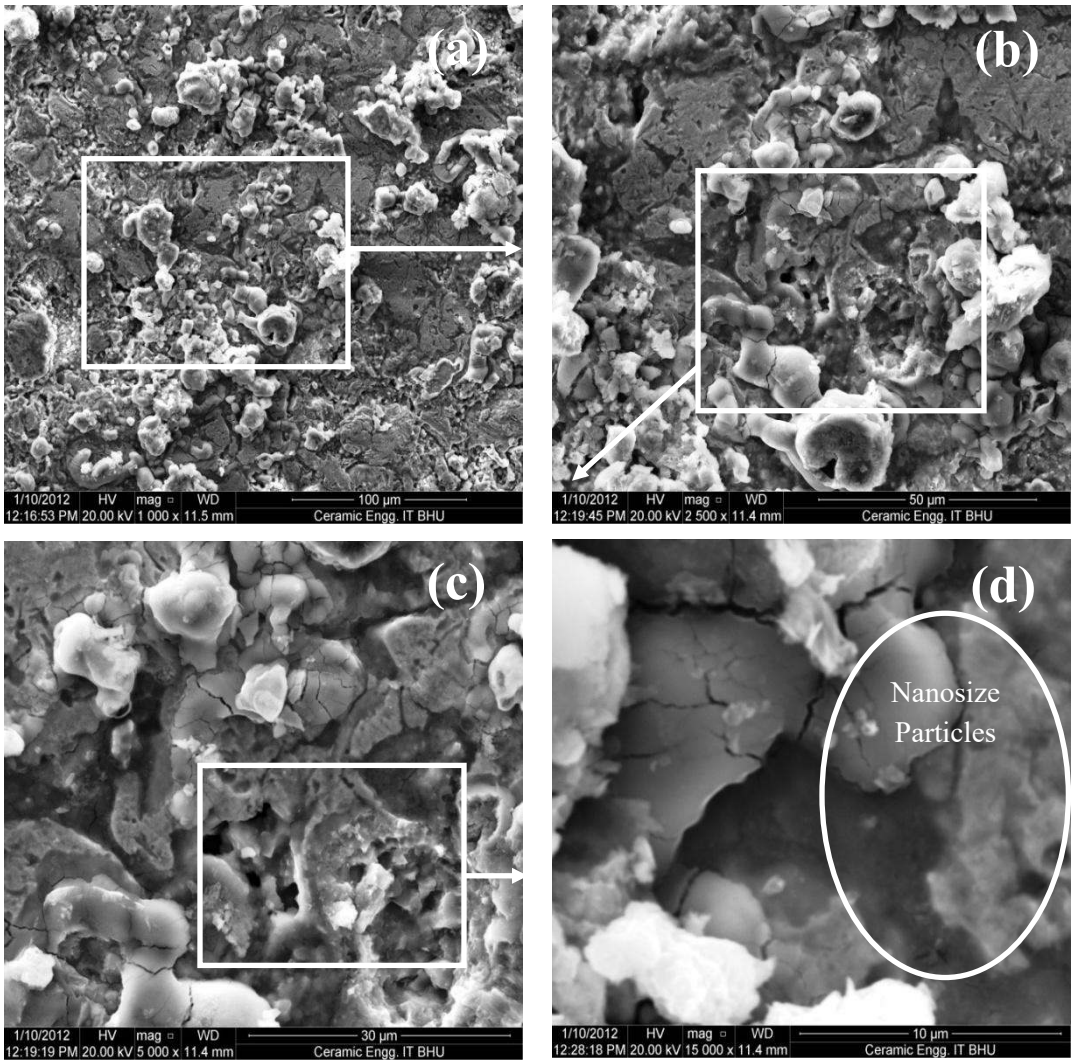

Fig. 7.2 SEM micrographs of 10AFe0.5Co1100(1) (a) 1000X magnification of the test specimen (b) 2500X magnification of circled portion in (a) (c) 5000X magnification of circled portion in (b) and (d) 15000X magnification of circled portion in (c); the circled portion show nanosize particles

In Fig. 7.2(c) and (d) some Fe, Al_2O_3 and CoO particles of sub micrometer size and of nanometer size are observed which formed during sintering phenomena. SEM micrograph for the specimen 10AFe1.0Co1100(1) is shown in Fig. 7.3(a), at 1000X. Formation of dense Fe-Al_2O_3-CoO metal matrix composite is seen. In Fig. 7.3 (b) it can be seen that the larger black grains are of iron, white are of alumina whereas the rest of the grains are of cobalt oxide which is present on the periphery of the grains of iron itself.

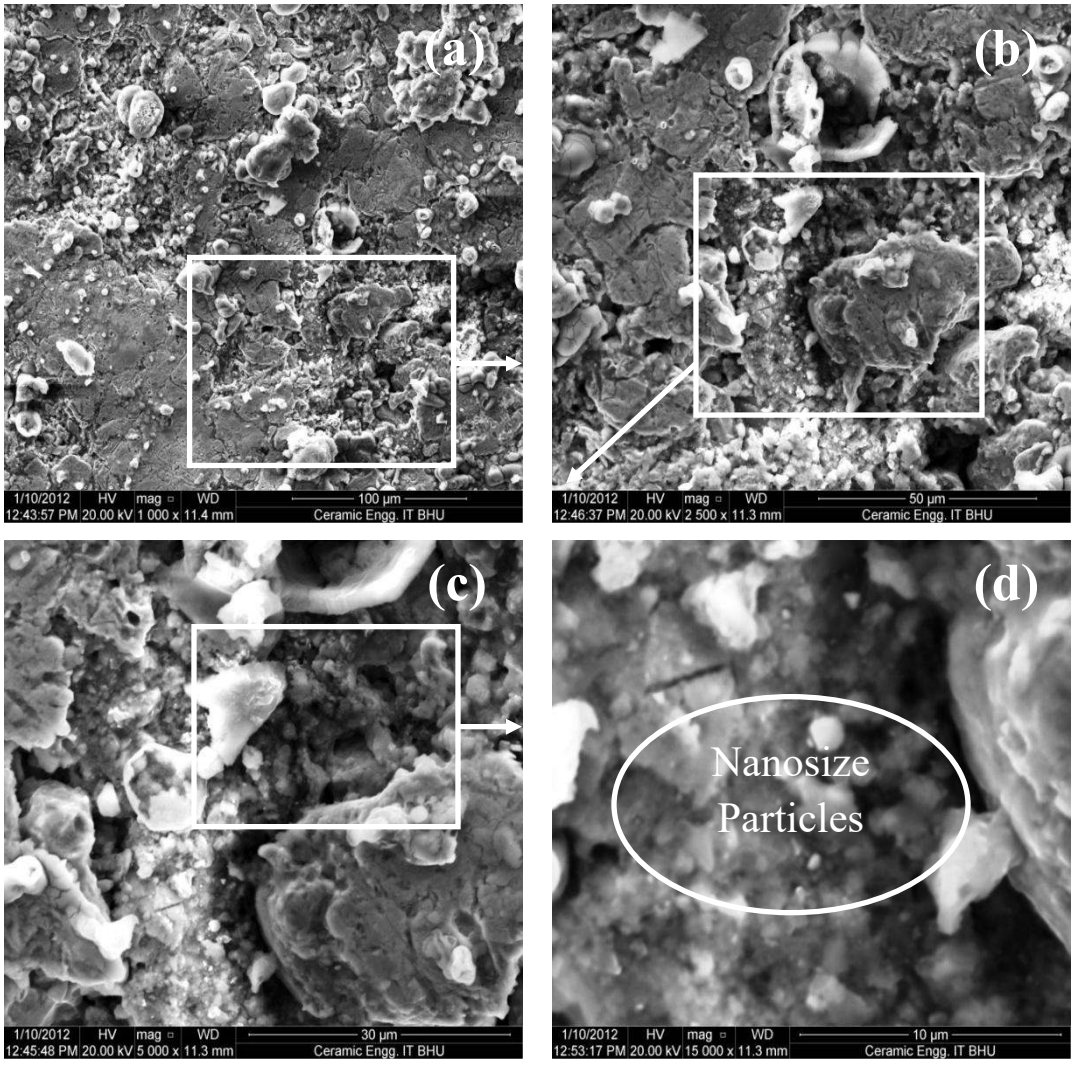

Fig. 7.3 SEM micrograph of 10AFe1.0Co1100(1) (a) 1000X magnification of the test specimen (b) 2500X magnification of circled portion in (a) (c) 5000X magnification of circled portion in (b) and (d) 15000X magnification of circled portion in (c); the circled portion show nanosize particles

In Fig. 7.3 (c) the Fe, Al_2O_3 and CoO particles are seen which are of sub micrometer size and of nanometer size which are formed during sintering process. The nanometer size particles are in the range of 45-60 nm which can be very easily seen in Fig. 7.3(d). On increasing the percentage of cobalt oxide finer grains of constituent phases are formed which can also be seen in Fig. 7.3(d). The bonding strength between the various grains is also reduced.

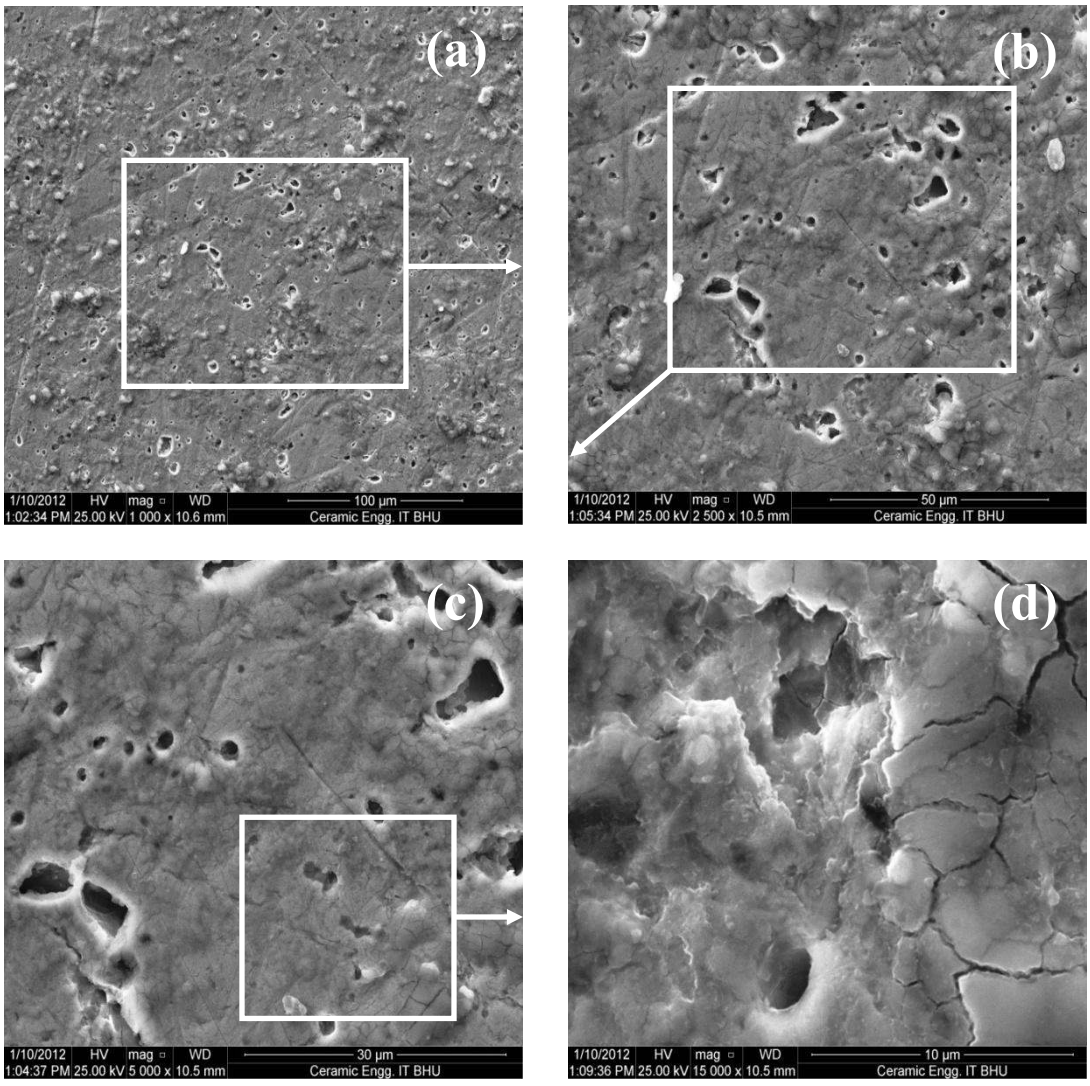

Fig. 7.4 SEM micrograph of Pure Fe + 0.5% CoO (a) 1000X magnification of the test specimen (b) 2500X magnification of circled portion in (a) (c) 5000X magnification of circled portion in (b) and (d) 15000X magnification of circled portion in (c); the circled portion show nanosize particles

SEM micrograph of the specimen pure Fe + 0.5% CoO is shown in Fig. 7.4. Figs. 7.4(a-b) show the scanning electron micrograph at 1000X and 2500X magnification which reveals the formation of dense Fe metal matrix composite with some porosity entrapped between grains. Figs. 7.4 (b-c) with increased magnifications show that the Fe particles are of sub micrometer and nanometer size. These are formed during sintering process. The nanometer size particles are in the range of 40-60 nm which can be very easily seen in Fig. 7.4(d) at 15000X magnification.

7.1.3 Density

Table 7.1 shows the green and the sintered densities of various CoO doped specimens. The green density of the specimen 10AFe0.5Co1100(1) was found to be 4.112 gm/cm^3 whereas the density after sintering was found to be 4.219 gm/cm^3. On adding 1.0% of cobalt oxide to the above composite composition, the specimen 10AFe1.0Co1100(1) show green density, 4.094 and upon sintering the specimen showed sintered density value of 4.160 gm/cm^3. The specimen 10AFe1.0Co1100(1) showed green density 4.099 gm/cm^3 and sintered density value of 4.155 gm/cm^3. For comparison purpose pure Fe+0.5% CoO was prepared, the specimen showed green density value of 4.619 gm/cm^3 and sintered density value of 4.968 gm/cm^3. Similarly a pure Fe specimen was made having green density of 4.728 gm/cm^3 and sintered density of 5.030 gm/cm^3.

It was found from the above discussion that there was a reduction in the green and sintered densities of the CoO doped Fe-Al_2O_3 nanocomposite specimens in comparison to that of iron-alumina based specimens. Specimen 10AFe1100(1) showed the green density value of 4.470 gm/cm^3. The reduction in the density values can be attributed due to the reduction in the iron aluminate phase formation as observed from the X-ray diffraction studies. The sintered density of P/M processed pure iron specimen (5.030 gm/cm^3) is highest. With CoO doping the density decreases due to entrapment of pores during sintering.

7.1.4 Hardness

The hardness of the specimens was measured on H scale. The hardness of the specimen on H scale for 10AFe0.5Co1100(1) was found to be 43 and that of 10AFe1.0Co1100(1) was found out to be 38. Table 7.1 also shows the hardness of different specimens on H Scale. These values of the hardness numbers were low as compared to the hardness number of the Fe-Al_2O_3 composite specimens. The hardness number of the specimen of pure iron was found to be 48 whereas it is 45 for specimens having pure iron with 0.5% CoO. The hardness values of specimen 10AFe0.5Co1100(1) and 10AFe1.0Co1100(1) were less in comparison to the specimen 10AFe1100(1).The hardness number reduced with increase in the percentage of CoO doping. The hardness number of the specimens reduced and it was seen that the hardness was less in comparison to the pure iron specimen. Specimen 10AFe1.0Co1100(1) showed the presence of finer nano size grains in comparison to 10AFe0.5Co1100(1). Due to the presence of finer nano size particles density value was also found to be reduced for the specimen 10AFe1.0Co1100(1) in comparison to to the specimen 10AFe0.5Co1100(1). Due to the reduction in the density value the hardness value was also found to be reduced. The hardness value of the specimens was found to be reduced on increasing the percentage of cobalt oxide content.

Table 7.1: Green, Sintered Density and Hardness of CoO doped specimens

S. No.	Sample Code	Green Density (gm/cm^3)	Sintered Density (gm/cm^3)	Hardness (HRH)
1.	10AFe0.5Co1100(1)	4.112	4.219	43
2.	10AFe1.0Co1100(1)	4.099	4.155	38
3.	Pure Fe+0.5% CoO	4.619	4.968	45
4.	Pure Fe	4.728	5.030	48

7.1.5 Wear

Fig. 7.5 shows the wear rate vs. load plots for the specimens 10AFe0.5Co1100(1) 10AFe1.0Co1100(1) and pure Fe+0.5% CoO. For specimen 10AFe0.5Co1100(1) the wear rates under lower loads, 0.5, 1.0 and 1.5 kg were found to be 0.2246, 0.2951 and 0.2967 mm^3/km respectively. For load greater than 1.5 kg i.e. at 2.0 kg the wear rate was found to be 1.6444 mm^3/km, which is much higher in comparison with the wear at lower loads. Specimen 10AFe1.0Co1100(1) at 0.5 kg load showed wear rate of 0.0784 mm^3/km, the value of wear rate increased to 0.6911 mm^3/km at load of 1.0 kg and this value reached 0.9299 mm^3/km at a load of 1.5 kg. Finally after measurement under this load, the specimen failed when tested under load of 2.0 kg. However, the wear rate of the specimen pure Fe+0.5% CoO at 0.5, 1.0, 1.5 and 2.0 kg load was found out to be 0.3133 mm^3/km, 0.3456 mm^3/km, 0.9876 mm^3/km and 1.8888 mm^3/km respectively.

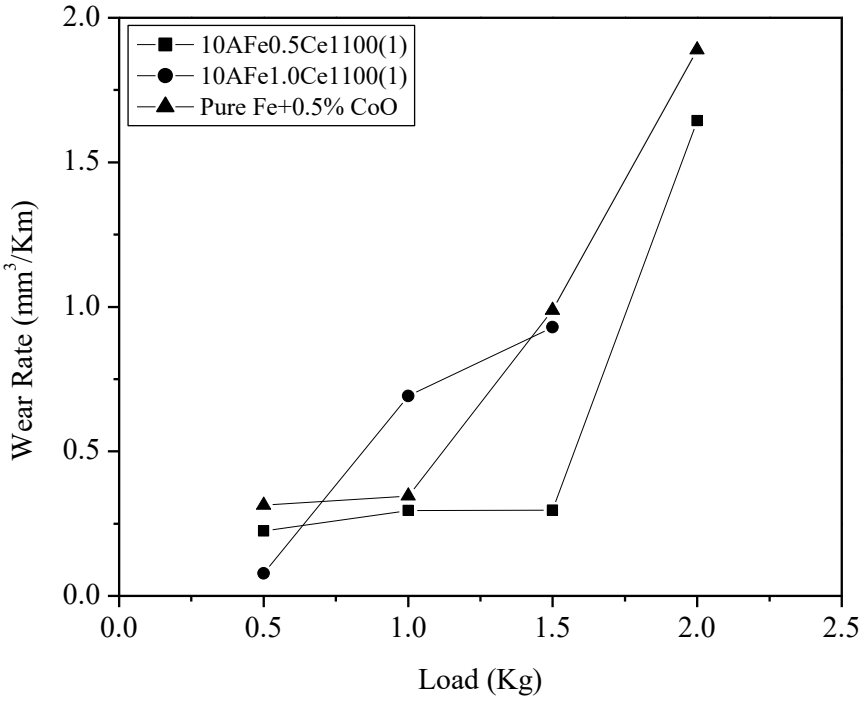

Fig. 7.5 Wear Rate vs. Load plot for specimen (a) 10AFe0.5Co1100(1) (b) 10AFe1.0Co1100(1) and (c) Pure Fe+0.5% CoO

The overall variation of wear rate with the load for different specimens can be explained as: The wear behavior of Fe-Al_2O_3 MMNC system has been reported by us earlier (Chapter 6). It has been found that two types of wear mechanism dominates in this system; adhesive and abrasive. Adhesive wear takes place at lower loads whereas abrasive wear dominates at higher loads. For the specimen 10AFe0.5Co1100(1) upto load of 1.5 kg, the adhesive wear occurred but at 2.0 kg load the wear behavior was abrasive in nature. The specimen 10AFe1.0Co1100(1) showed the abrasive wear under all loads. It appears that the bonding between different particles in the composite specimen is small and particles come in between the specimen and the disc causing abrasive wear even under lower loads. This may also be the reason for failure of the specimen during wear test at 2.0 kg load.

Fig. 7.6 shows the SEM of the specimen 10AFe0.5Co1100(1) after wear test at (a) 500X (b) 5000X and (c) 20,000X. Fig. 7.6 (a) shows the SEM of worn out specimen at 500X after testing at a load of 2.0 kg. This micrograph shows presence of scoring marks on the specimen surface. The removal of the material from the specimen surface is due to the entrapment of hard alumina particles between the disc and the pin surface. SEM of the same specimen at 5000X is shown in Fig 7.6 (b). The present micrograph illustrates the removal of the material by adhesion in the starting i.e. upto a load of 1.5 kg while at 2.0 kg load it showed abrasive wear. This observation can be clearly seen in the present micrograph which shows the smoothened surface at some place whereas at some places the abraded particles can be seen. The same specimen when viewed at 20,000X as shown in Fig. 7.6 (c) shows the nano size particles of Fe and Al_2O_3 respectively.

Fig. 7.7 shows the SEM of the specimen 10AFe1.0Co1100(1) after wear test at (a) 500X (b) 5000X and (c) 20,000X. Fig. 7.7(a) shows the SEM of the specimen after wear test upto 1.5 kg taken at a magnification of 500X. The present micrograph shows some slight wear marks along with some irregular shaped peel type structure present on the pin surface. The specimen failed after a load of 1.5 kg.

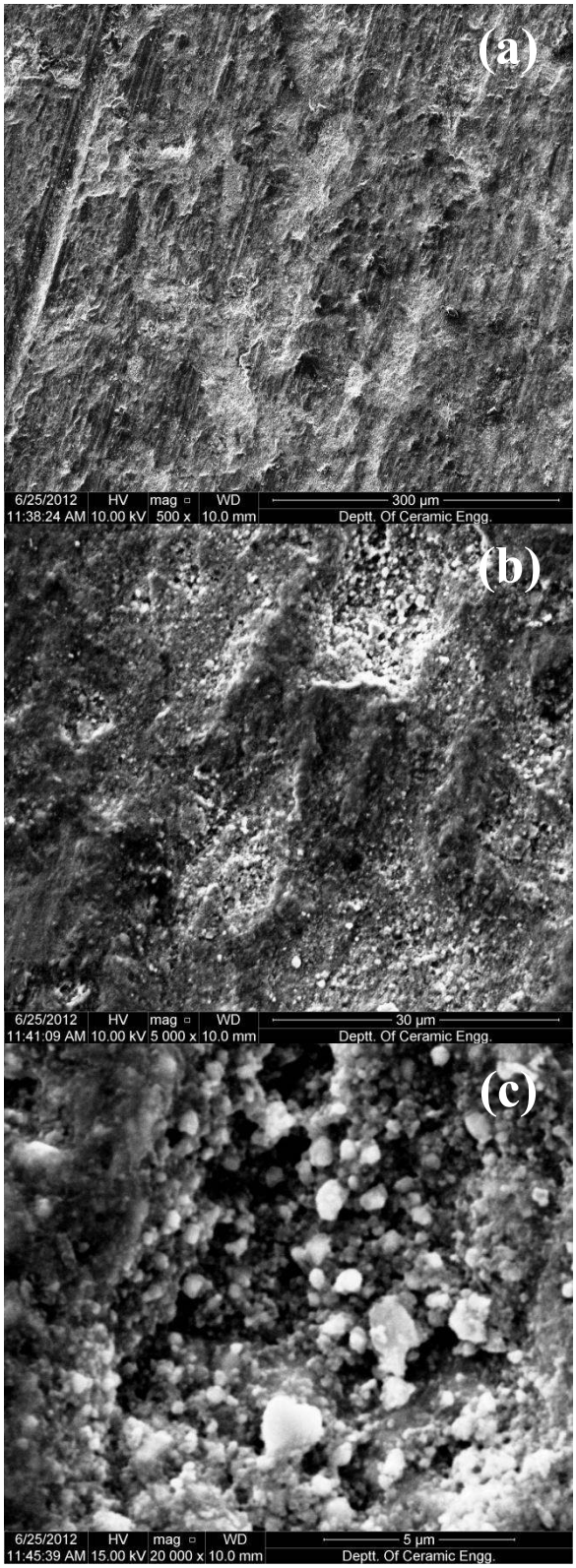

Fig. 7.6 SEM of specimen 10AFe0.5Co1100(1) after wear test (a) 500X (b) 5000X and (c) 20000X

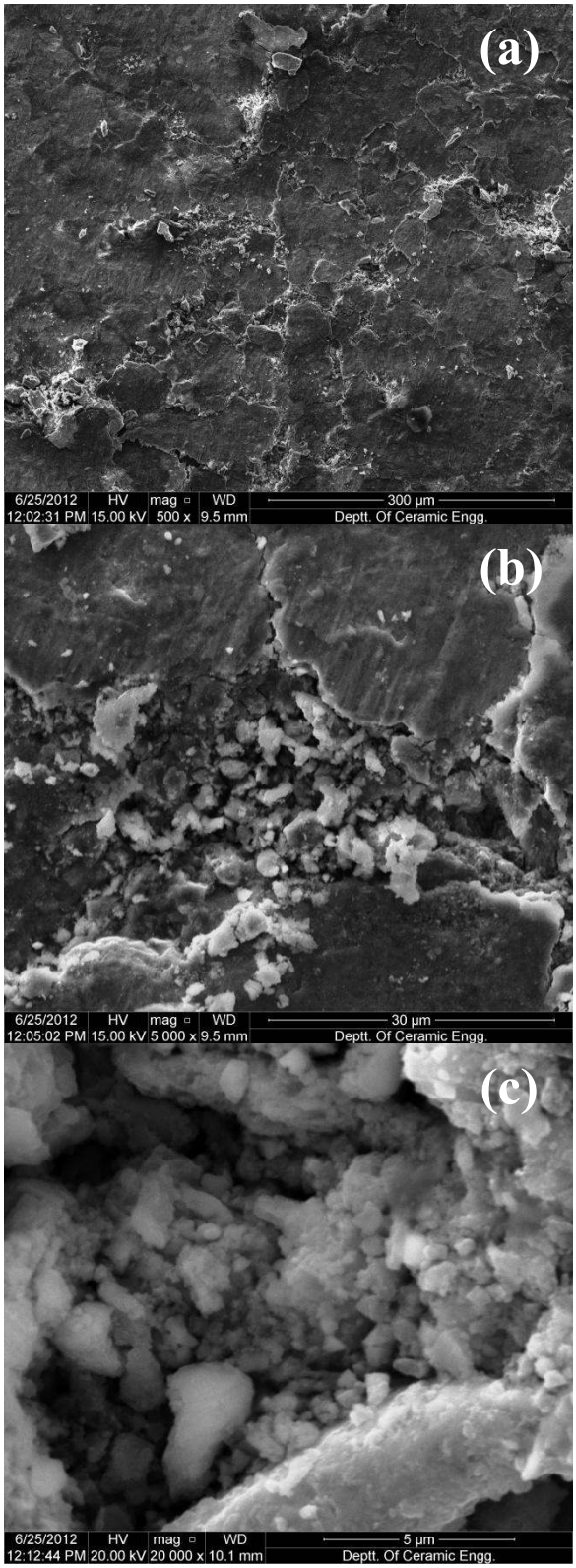

Fig. 7.7 SEM of specimen 10AFe1.0Co1100(1) after wear test (a) 500X (b) 5000X and (c) 20000X

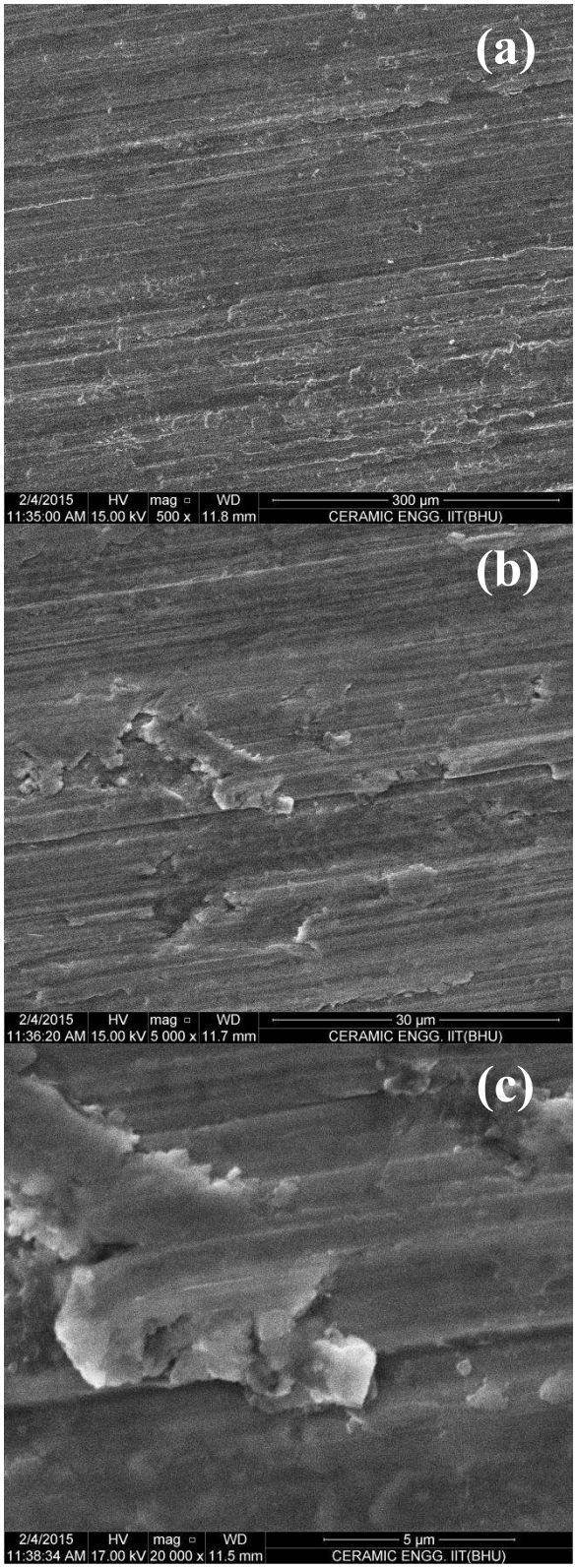

Fig. 7.8 SEM of specimen Pure Fe+0.5% CoO after wear test (a) 500X (b) 5000X and (c) 20000X

Fig. 7.7(b) shows the SEM of same specimen at 5000X which illustrates that the removal of the material from the pin surface was abrasive from starting and therefore there is a smoothing as well as digging effect present on the specimen surface itself. The digging action is due to the tribo film formation between the pin and disc surface. The overall wear rate was quite low which is attributed to the formation of nano size particles of Fe and Al_2O_3 which are seen in the micrograph of the same specimen at 20,000X [Fig. 7.7(c)].

Fig. 7.8 shows the SEM of the specimen pure Fe+0.5% CoO after wear test at (a) 500X (b) 5000X and (c) 20,000X. Fig. 7.8(a) shows the SEM of the specimen after wear test upto 2.0 kg taken at a magnification of 500X. The present micrograph illustrates light tangential skiving marks on the entire surface of the specimen with the presence of no grooves. The same specimen when viewed at a magnification of 5000X reveals the adhesive wear marks on the specimen surface. It also shows some peeled off material from the parent surface. Fig. 7.8(c) shows the SEM image of the specimen at 20000X revealing the presence of adhesive layer on the surface of the specimen.

7.2 CeO_2 Doped Fe-Al_2O_3 Metal Matrix Nanocomposites

Composition of the composite was 90% Fe and 10% Al_2O_3 by weight, 0.5 and 1.0% by weight of the cerium oxide (CeO_2) was used as the dopant in this composite system. Appropriate mixtures of Fe, Al_2O_3, CeO_2 and dextrin (binder) were ball milled using zirconia balls as the grinding and mixing media with powder to ball ratio as 1:2. The composition was dry ball milled for 2 hours. The mixed composition was compacted in a die of 16 mm diameter under a load of 7 tons. Sintering of the green compacts was carried out in an argon atmosphere at 1100°C for 1h. After sintering, the compacts were machined. It was found that the machinability of the specimens was better than the un-doped specimens. Initially the dimensions of the specimen were 22 mm height and 16 mm diameter, after the sintering process and after machining the dimensions of the specimens were 20 mm height and 12 mm diameter

respectively. Thereafter, the surface of the specimens was polished. A nomenclature e.g. 10AFe0.5Ce1100(1) is given to each specimen. Here A denotes the aluminum oxide, Fe denotes iron, 0.5Ce denotes the percentage of cerium oxide, 1100 denotes the sintering temperature, 1 denotes time of sintering time in hr.

7.2.1 X-ray Diffraction

Fig. 7.9 shows XRD patterns of the specimen (a) 10AFe0.5Ce1100(1) (b) 10AFe1.0Ce1100(1) and (c) pure Fe+0.5% CeO_2. All the characteristics peaks of the specimens were indexed with the JCPDS data file to identify the corresponding phases. In the specimen 10AFe0.5Ce1100(1) it was found that iron (Fe), aluminium oxide (Al_2O_3), iron aluminate ($FeAl_2O_4$) and cerium oxide (CeO_2) phases are present. It was found in the present specimen that reaction takes place between iron and aluminium oxide particles due to which iron aluminate phase forms whereas, cerium oxide is present as a separate phase.

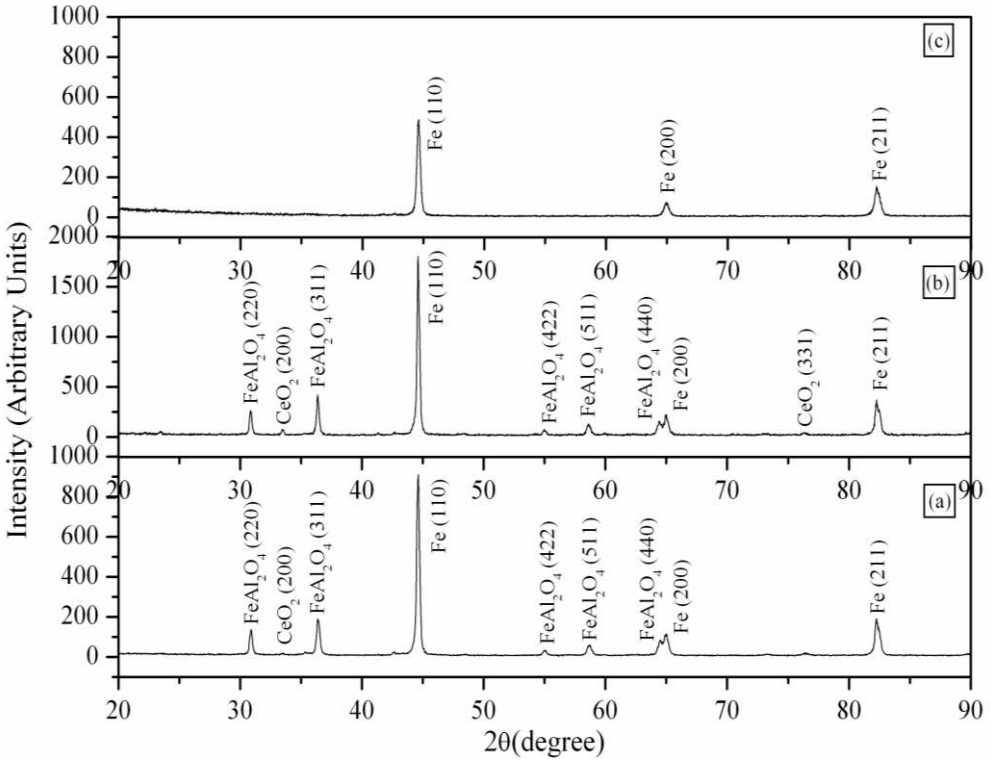

Fig. 7.9 XRD pattern of specimen (a) 10AFe0.5Ce1100(1) (b) 10AFe1.0Ce1100(1) and (c) Pure Fe+0.5% CeO_2

Similarly, specimen 10AFe1.0Ce1100(1) also shows the presence of iron (Fe), aluminium oxide (Al_2O_3), iron aluminate ($FeAl_2O_4$) and cerium oxide (CeO_2) phases respectively. Iron aluminate phase in the present case also forms due to the reactive sintering whereas the cerium oxide is present as a separate phase. It can be seen that the amount of the cerium oxide phase is more in the specimen 10AFe1.0Ce1100(1) in comparison to the specimen 10AFe0.5Ce1100(1). Specimen having pure iron doped with 0.5% CeO_2 showed the presence of only iron phase. It was also found that the intensity of iron phase was also reduced by adding the cerium oxide into it.

7.2.2 Scanning Electron Microscopy

Fig. 7.10 shows the scanning electron micrographs of the specimen 10AFe0.5Ce1100(1) at (a) 200X (b) 1000X (c) 5000X and (d) 10000X respectively. Fig. 7.10(a) shows the electron microscopic image of the specimen at 200X which shows dense phase microstructure with the presence of negligible amount of porosity. Fig. 7.10(b) shows the electron microscopic image of the same specimen at 1000X which shows the particles of iron (Fe), aluminium oxide (Al_2O_3), iron aluminate ($FeAl_2O_4$) and some trace amount of cerium oxide (CeO_2). The same micrograph when viewed at 5000X (Fig. 7.10(c)) shows the presence of dense phase iron aluminate with the presence of the cerium oxide particles present in the intergranular site of the nanocomposite structure. The same micrograph also shows some circular shaped alumina particles. Fig. 7.10(d) shows the SEM image of the same specimen at 10000X illustrating the presence of nano size particles of iron aluminate phase along with the presence of cerium oxide particles in the intergranular pores of the nanocomposite specimen.

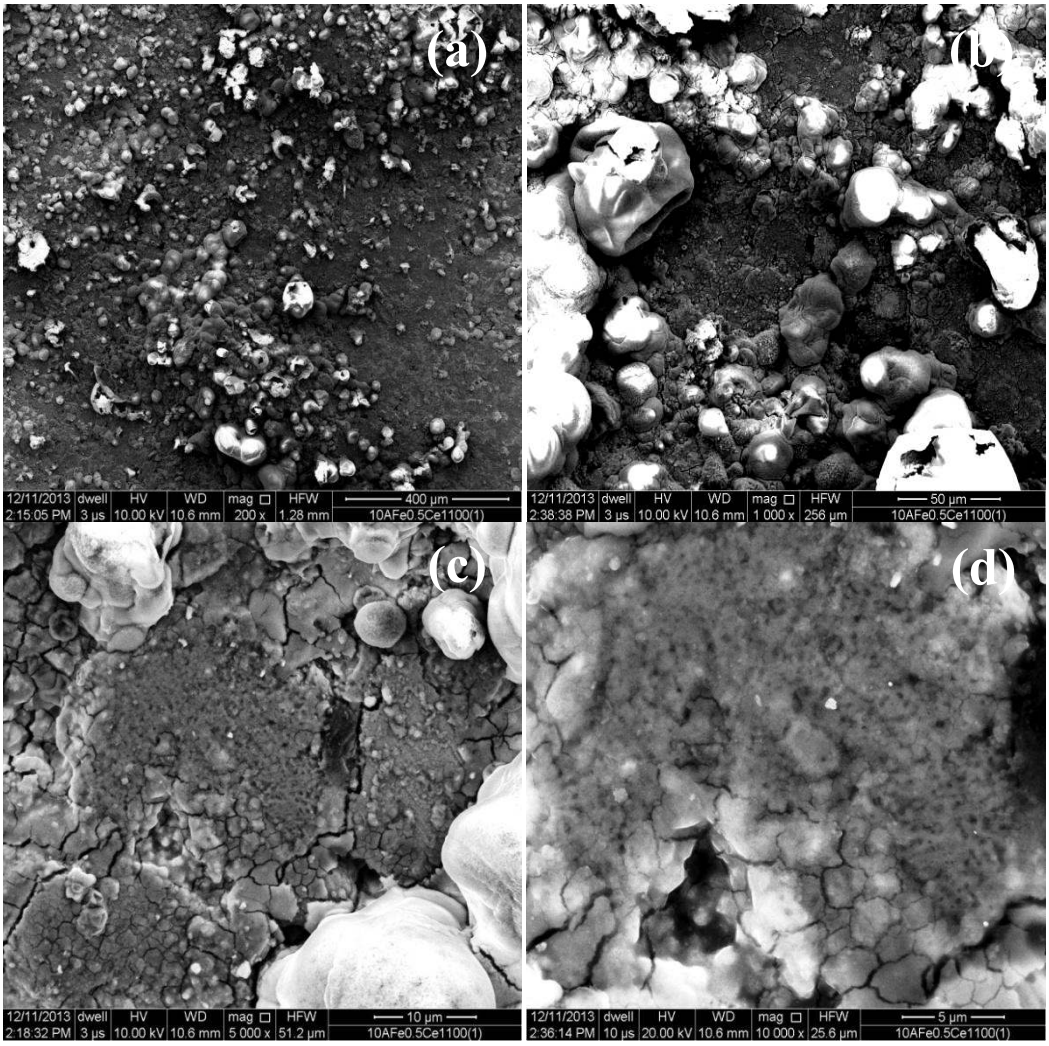

Fig. 7.10 SEM of 10AFe0.5Ce1100(1) at (a) 200X (b) 1000X (c) 5000X and (d) 10000X respectively

Fig. 7.11 shows the scanning electron micrographs of the specimen 10AFe1.0Ce1100(1) at (a) 200X (b) 1000X (c) 5000X and (d) 10000X respectively. Fig. 7.11(a) shows the scanning electron micrograph of the specimen at 200X revealing the formation of highly dense phase structure with the presence of negligible amount of porosity. Fig. 7.11(b) shows the SEM micrograph of the same specimen at 1000X which shows the particles of iron, alumina, iron aluminate and cerium oxide respectively. Bigger size particles of size 5-10 µm are of iron, circular particles of size 4-8 µm can be seen very easily in the present micrograph. The same specimen when viewed at 5000X (Fig. 7.11(c)) shows the presence of nano size

grains of iron aluminate phase present in the intergranular and intragranular pores of the nanocomposite specimen. Some nano size particles of cerium oxide are also present in the intergranular pores of the nanocomposite specimen. Fig. 7.11(d) shows the scanning electron micrograph of the same specimen at 10000X which clearly depicts the formation of nano iron aluminate particles on bigger grains of iron. At some places nano rods have also formed inside the particles due to the reaction between iron and alumina particles along with some interaction of cerium oxide particles.

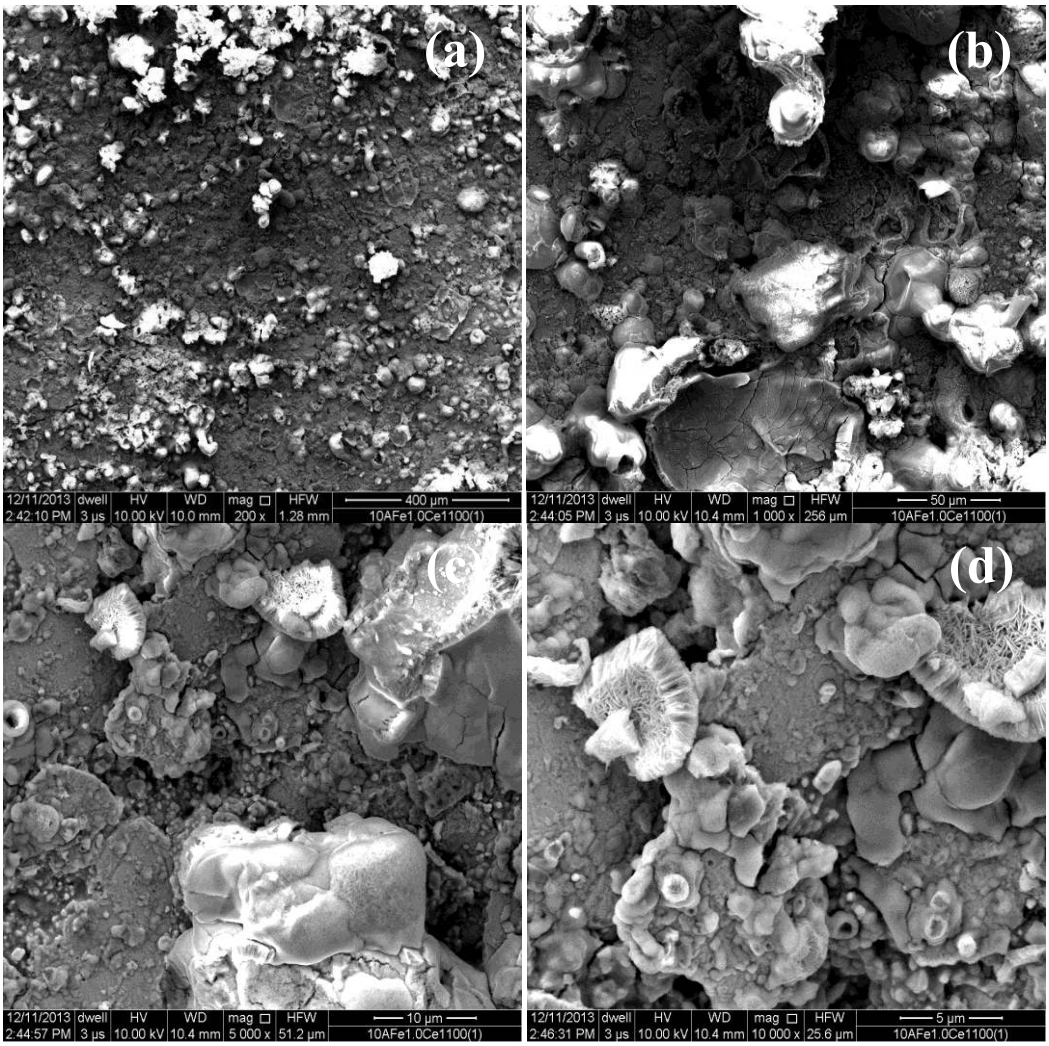

Fig. 7.11 SEM of 10AFe1.0Ce1100(1) at (a) 200X (b) 1000X (c) 5000X and (d) 10000X respectively

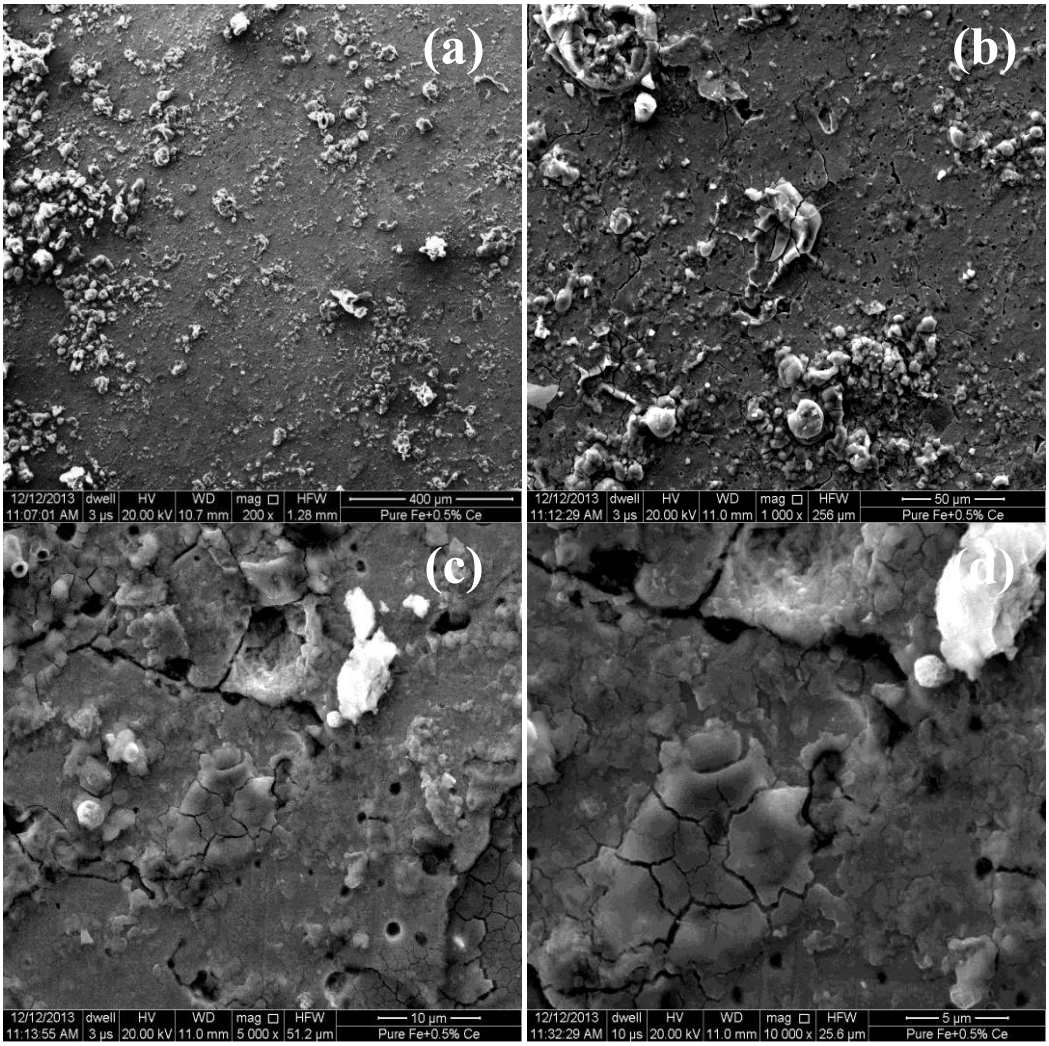

Fig. 7.12 SEM of Pure Fe+0.5% CeO_2 at (a) 200X (b) 1000X (c) 5000X and (d) 10000X respectively

Fig. 7.12 shows the SEM of Pure Fe+0.5% CeO_2 specimen at (a) 200X (b) 1000X (c) 5000X and (b) 10000X respectively. Fig. 7.12(a) shows the scanning electron micrograph of the specimen at 200X revealing a highly dense phase structure with some minute amount of porosity. It can be seen in the same micrograph that the some particles of cerium oxide are present on the upper bound surface of the specimen. The same micrograph when viewed at 1000X (Fig. 7.12(b)) revealed the presence of some intragranular porosity on the specimen surface. There is no reaction between the various powders due to the entrapment of the cerium oxide particles. Fig. 7.12(c) shows the SEM of the same specimen at 5000X which shows some minute

intragranular pores of size 1-2 µm. The same specimen when viewed at 10000X [Fig. 7.12(d)] shows the nano size particles of cerium oxide in the intergranular pores of the specimen. From the above discussion on SEM micrographs, it can be concluded that the density of the specimen with 1% of cerium oxide dopant was found to be the highest.

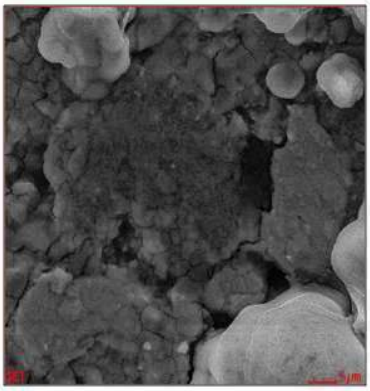

(a)

Element	Wt%	At%
OK	12.01	30.82
AlK	05.69	08.66
ClK	00.94	01.09
CeL	00.83	00.24
FeK	80.52	59.18
Matrix	Correction	ZAF

(c)

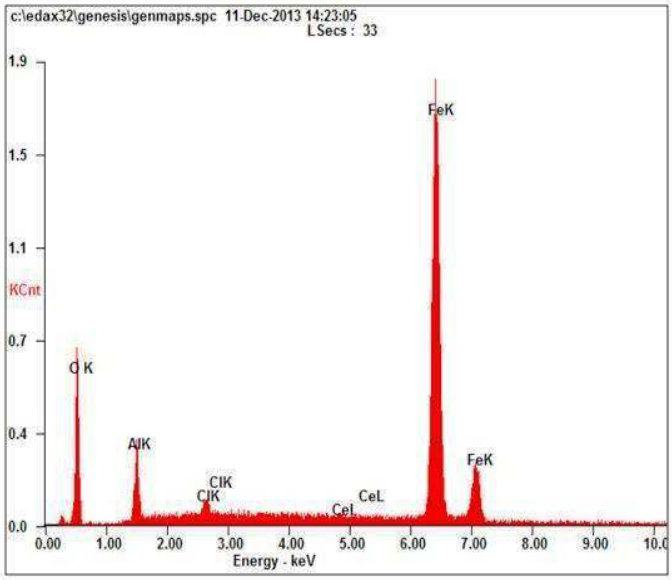

(b)

Fig. 7.13 Full frame microscopic investigation of specimen 10AFe0.5Ce1100(1) (a) SEM image (b) full frame EDAX (c) elemental profile at 10000X

Fig. 7.13 shows the full frame microscopic investigation of the specimen 10AFe0.5Ce1100(1) (a) SEM image (b) full frame EDAX (c) elemental profile. Full frame shows the presence of oxygen, aluminium, chlorine, cerium and iron. It was found from the above investigation that oxygen is 12.01 wt%, aluminium is 05.69 wt%, chlorine is 00.94 wt%, cerium is 00.83 wt% and iron is 80.52 wt% respectively. Thus, it can be concluded that in the full frame view all the elements were present.

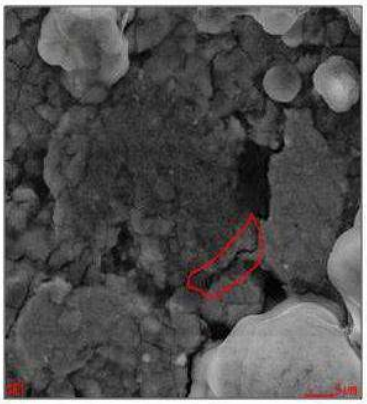

(a)

Element	Wt%	At%
CK	06.04	15.25
OK	17.91	33.95
AlK	16.65	18.71
ClK	00.54	00.46
CeL	01.03	00.22
FeK	57.83	31.40
Matrix	Correction	ZAF

(c)

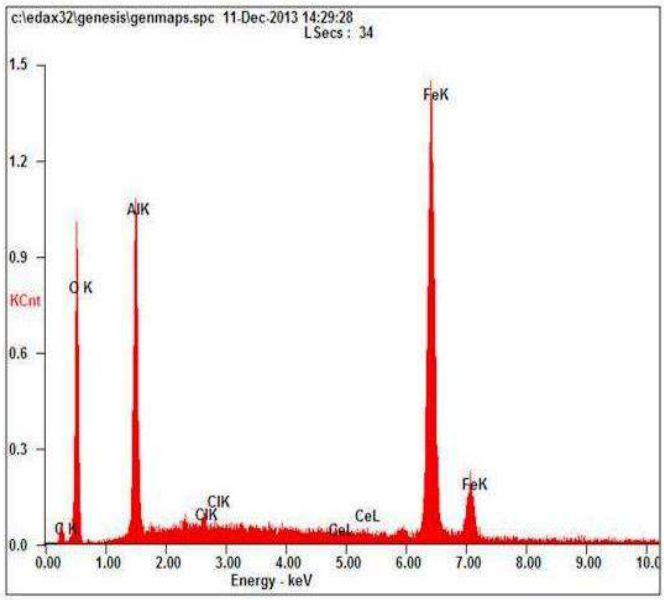

(b)

Fig. 7.14 Regional microscopic investigation of specimen 10AFe0.5Ce1100(1) (a) SEM image (b) full frame EDAX (c) elemental profile at 10000X

Fig. 7.14 shows the regional microscopic investigation of the specimen 10AFe0.5Ce1100(1) (a) SEM image (b) full frame EDAX (c) elemental profile. Various elements present in the composition were carbon, oxygen, aluminium, chlorine, cerium and iron. Carbon is 06.04 wt%, oxygen is 17.91 wt%, aluminium is 16.65 wt%, chlorine is 00.54 wt%, cerium is 01.03 wt% and iron is 57.83 wt% respectively. The presence of carbon is due to removal of dextrin during the sintering process which gets entrapped in the pores of the specimens. It was also found that the percentage of cerium was high in the intergranular porosity of the specimen. The presence of carbon indicates that some residue of binder (dextrin) burn out remains in the specimen in the form of carbon. It implies that complete burn out of dextrin is not taking place at sintering temperature under inert atmosphere.

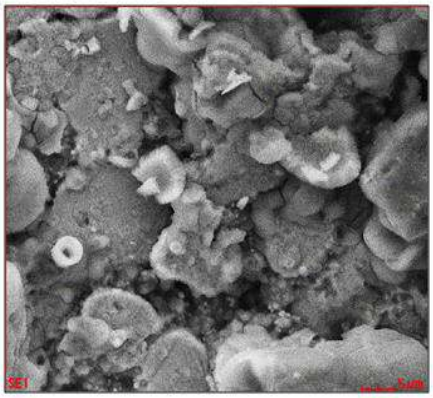

(a)

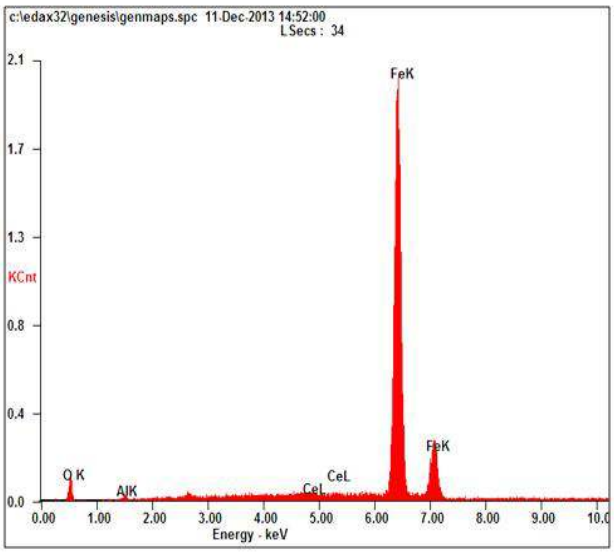

(b)

Element	Wt%	At%
OK	02.18	07.24
AlK	00.52	01.02
CeL	01.29	00.49
FeK	96.01	91.25
Matrix	Correction	ZAF

(c)

Fig. 7.15 Full frame microscopic investigation of specimen 10AFe1.0Ce1100(1) (a) SEM image (b) full frame EDAX (c) elemental profile at 10000X

Fig. 7.15 shows the full frame microscopic investigation of the specimen 10AFe1.0Ce1100(1) (a) SEM image (b) full frame EDAX (c) elemental profile. Energy dispersive spectroscopy shows the presence of oxygen, aluminium, cerium and iron. In the present view oxygen is 02.18 wt%, aluminium is 00.52 wt%, cerium is 01.29 wt% and iron is 96.01 wt% respectively. On the basis of the above investigation it was found that all the constituent elements were present in the nanocomposite specimen.

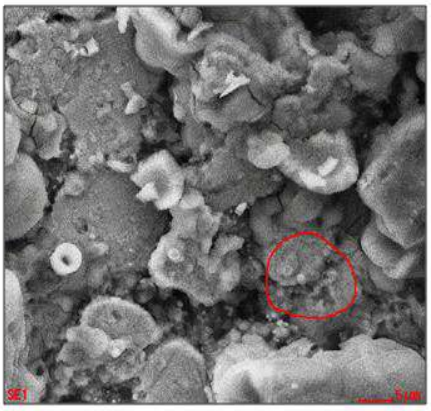

(a)

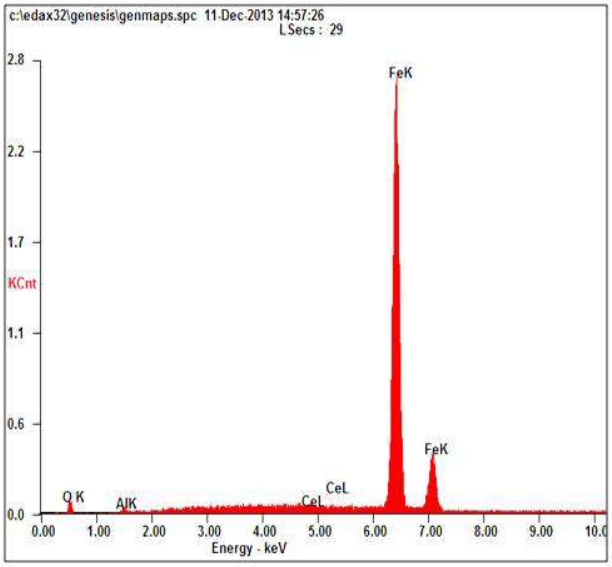

(b)

Element	Wt%	At%
OK	01.30	04.38
AlK	00.63	01.26
CeL	00.55	00.21
FeK	97.52	94.15
Matrix	Correction	ZAF

(c)

Fig. 7.16 Regional microscopic investigation of specimen 10AFe1.0Ce1100(1) (a) SEM image (b) full frame EDAX (c) elemental profile at 10000X

Fig. 7.16 shows the regional microscopic investigation of specimen 10AFe1.0Ce1100(1) (a) SEM image (b) full frame EDAX (c) elemental profile. Regional investigation shows the presence of oxygen, aluminium, cerium and iron respectively. In the present view oxygen is 01.30 wt%, aluminium is 00.63 wt%, cerium is 00.55 wt% and iron is 97.52 wt% respectively. In this micrograph all the elements are present which were mixed initially.

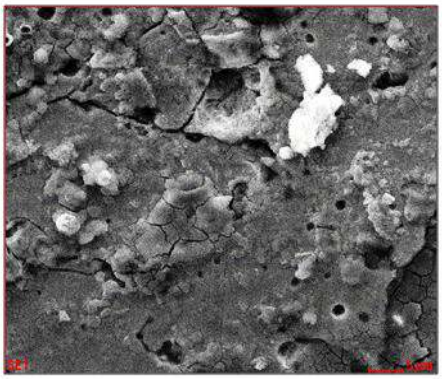

(a)

Element	Wt%	At%
OK	06.82	20.42
CeL	00.66	00.23
FeK	92.52	79.35
Matrix	Correction	ZAF

(c)

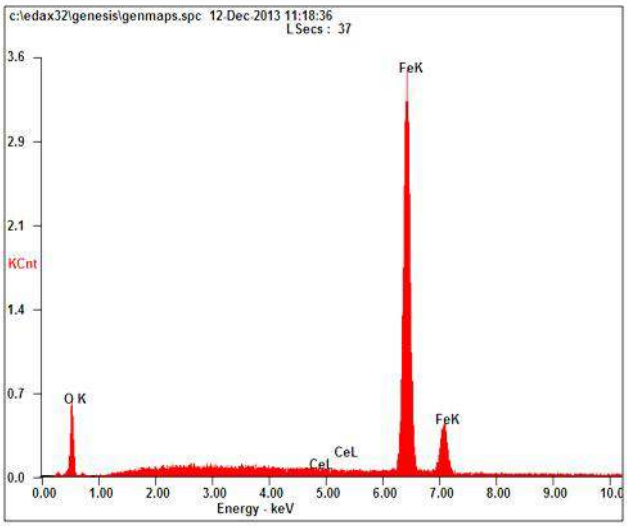

(b)

Fig. 7.17 Full frame microscopic investigation of specimen Pure Fe+0.5% CeO_2 (a) SEM image (b) full frame EDAX (c) elemental profile at 10000X

Fig. 7.17 shows full frame microscopic investigation of specimen Pure Fe+0.5% CeO_2 (a) SEM image (b) full frame EDAX (c) elemental profile. Full frame micrograph of the present specimen shows the presence of oxygen, cerium and iron respectively. In the present view oxygen is 06.82 wt%, cerium is 00.66 wt% and iron is 92.52 wt% respectively. All the elements are present in the stoichiometric ratio.

Fig. 7.18 shows the regional microscopic investigation of specimen pure Fe+0.5% CeO_2 (a) SEM image (b) full frame EDAX (c) elemental profile. Regional microscopic investigation of the present specimen shows the presence of oxygen, cerium and iron respectively. In the present view oxygen is 10.13 wt%, cerium is 00.69 wt% and iron is 89.18 wt% respectively. All the elements are present in the ratio as expected from the initial composition.

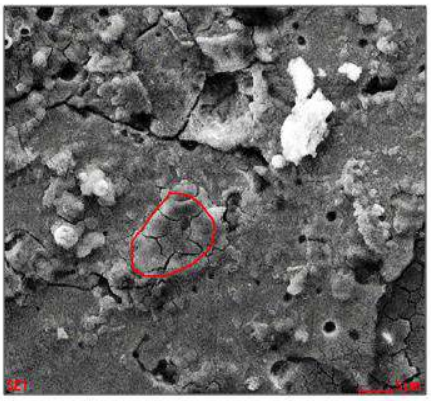

(a)

Element	Wt%	At%
OK	10.13	28.33
CeL	00.69	00.22
FeK	89.18	71.45
Matrix	Correction	ZAF

(c)

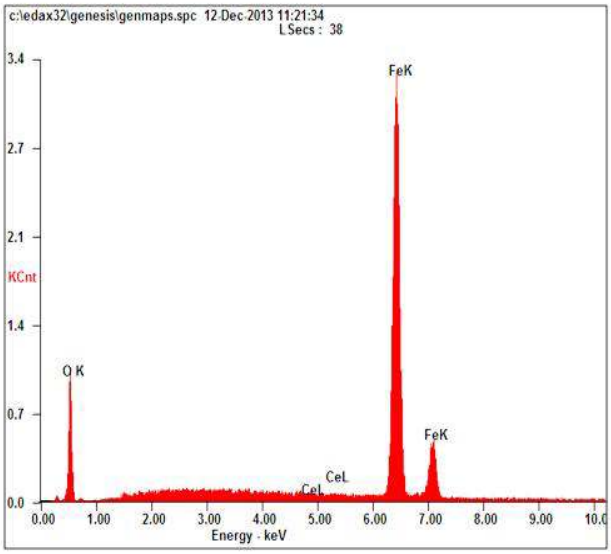

(b)

Fig. 7.18 Regional microscopic investigation of specimen Pure Fe+0.5% CeO_2 (a) SEM image (b) full frame EDAX (c) elemental profile at 10000X

7.2.3 Density

Table 7.2 illustrates the green density, sintered density and hardness of the synthesized nanocomposite specimens. In order to maintain the accuracy of measurement among the specimen's three specimens were prepared for each composition. Specimen 10AFe0.5Ce1100(1)-1,2,3 showed green density of 4.679, 4.657, 4.584 gm/cc and a sintered density of 4.6853, 4.6635, 4.6574 gm/cc. The mean green and sintered density value calculated for this specimen was found to be 4.640 gm/cc and 4.669 gm/cc respectively. On increasing the percentage of cerium oxide to 1.0% three specimens were fabricated namely 10AFe1.0Ce1100(1)-1,2,3 which showed green density values of 4.659, 4.827 and 4.700 gm/cc. On sintering these specimens the sintered density values of these three specimens was found out to be

4.701, 4.898 and 4.777 gm/cc. The mean green and sintered density value for the specimen 10AFe1.0Ce1100(1) was found out to be 4.728 gm/cc and 4.792 gm/cc respectively. A few specimens with addition of 0.5% CeO_2 as the dopant in the iron matrix were also fabricated. These synthesized specimens showed green density of 5.195, 5.089 and 5.222 gm/cc whereas sintered density values of 5.310, 5.445 and 5.316 gm/cc respectively. The mean green and sintered density value for this specimen was found to be 5.169 gm/cc and 5.357 gm/cc respectively.

Table 7.2 Green Density, Sintered Density and Hardness of CeO_2 doped specimens

Sl. No.	Specimen Code	Green Density (gm/cm^3)	Sintered Density (gm/cm^3)	Hardness (HRH)
1.	10AFe0.5Ce1100(1)	4.640	4.669	70
2.	10AFe1.0Ce1100(1)	4.728	4.792	83
3.	Pure Fe+0.5% CeO_2	5.169	5.357	47
4.	Pure Fe	4.728	5.030	48

It was seen that in all the nanocomposite specimens the sintered density was more in comparison to the green density. From the above results it is concluded that on increasing the percentage of cerium oxide in the composite the density value also increases. Addition of 0.5% CeO_2 in the iron matrix also showed improvement in the density values. It is evident to note that the density value of 5AFe1100(1) and 10AFe1100(1) was 4.817 gm/cc and 4.471 gm/cc. 0.5% and 1.0% cobalt oxide doping in Fe-10% Al_2O_3 nanocomposite specimen showed density values of 4.236 gm/cc and 4.160 gm/cc respectively. Thus, density values for cerium oxide doped nanocomposite specimens were found to be higher in comparison to the pure and CoO doped Fe-Al_2O_3 nanocomposite specimens.

7.2.4 Hardness

Table 7.2 shows the mean hardness of the specimen. Specimens 10AFe0.5Ce1100(1)-1,2,3 showed hardness number of 73 HRH, 71 HRH and 67 HRH whereas specimen 10AFe1.0Ce1100(1)-1,2,3 showed hardness number of 79 HRH, 82 HRH and 87 HRH. Pure Fe specimen with 0.5% CeO_2 showed hardness number of 44, 52 and 46 respectively. The mean hardness values for the specimen 10AFe0.5Ce1100(1), 10AFe1.0Ce1100(1) and Pure Fe+0.5% CeO_2 was found out to be 70 HRH, 83 HRH and 47 HRH respectively. The hardness number of the specimen 5AFe1100(1) and 10AFe1100(1) was found to be 38 HRH and 26 HRH respectively. In the present nanocomposite specimens, two types of sintering behavior is observed; (i) solid state sintering between iron particles and (ii) reactive sintering between iron and aluminium oxide particles associated with the formation of iron aluminate. With first kind of sintering, there will be no change in the fraction of ceramic reinforcement in the nanocomposite and metallic characteristics are enhanced due to densification resulting in the decrease in hardness number, whereas with second kind of reactive sintering, content of aluminate phase i.e. ceramic phase, increases resulting in an increase in the hardness number. At higher sintering temperature i.e. 1100°C, reactive sintering rate increases due to formation of ceramic $FeAl_2O_4$ nano-particles resulting in an increase in hardness number of the nanocomposite specimen. Cerium oxide particles which are added in the nanocomposites specimens goes inside the pores and ultimately increases the hardness of the specimen. It is quite interesting to note that the hardness number of mild steel, cast iron and high carbon steel was found to be 12 HRH, 14 HRH and 16 HRH respectively. Thus, the hardness number of the synthesized nanocomposite specimens was found to improve significantly in comparison to the pure iron specimens

7.2.5 Wear

Fig. 7.19 shows the wear rate vs. load plots (a) 10AFe0.5Ce1100(1) (b) 10AFe1.0Ce1100(1) and (c) Pure Fe+0.5% CeO_2.

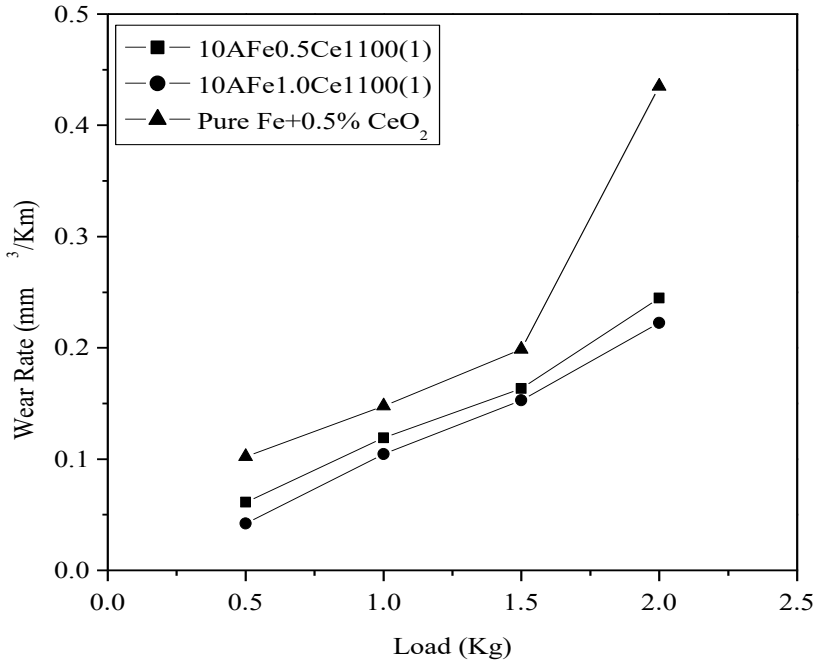

Fig. 7.19 Wear Rate vs. Load Plots (a) 10AFe0.5Ce1100(1) (b) 10AFe1.0Ce1100(1) and (c) Pure Fe+0.5% CeO_2

Specimen 10AFe0.5Ce1100(1) shows wear rate of 0.0612 mm^3/km at a load of 0.5 kg, 0.1192 mm^3km at a load of 1.0 kg, 0.1633 mm^3/km at a load of 1.5 kg and 0.2447 mm^3/km at a load of 2.0 kg. For specimen 10AFe1.0Ce1100(1) the wear rate of the specimen at a load of 0.5, 1.0, 1.5 and 2.0 kg load was found to be 0.0422, 0.1045, 0.1527 and 0.2223 mm^3/km respectively. Pure iron specimen having 0.5% CeO_2 showed wear rate of 0.1022 mm^3/km, 0.1476 mm^3/km, 0.1987 mm^3/km and 0.4349 mm^3/km at a load of 0.5, 1.0, 1.5 and 2.0 kg respectively. It was seen from the above results that on increasing the percentage of cerium oxide in the nanocomposite specimen the wear rate value were found to reduce however the pure iron specimen having 0.5% CeO_2 showed the highest wear rate values at all the loads.

Fig. 7.20 shows SEM images of specimen 10AFe0.5Ce1100(1) after wear test (a) 200X (b) 2,500X and (c) 10,000X.

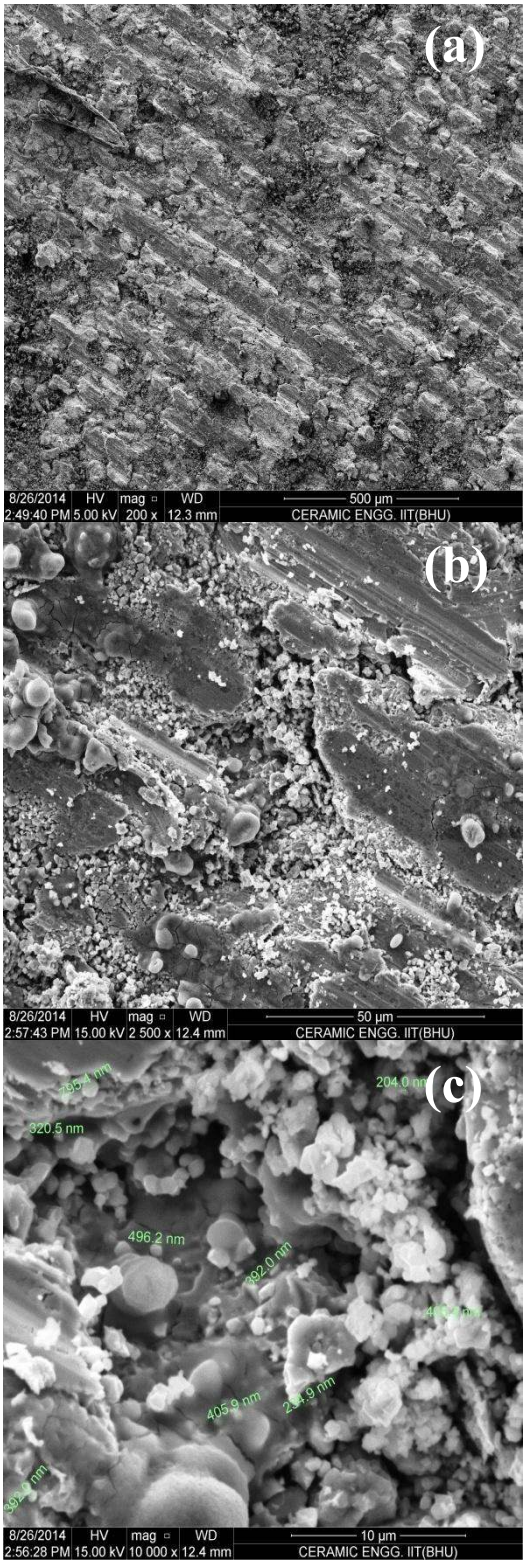

Fig. 7.20 SEM of worn specimen 10AFe0.5Ce1100(1) after wear test(a) 200X (b) 2500X and (c) 10000X

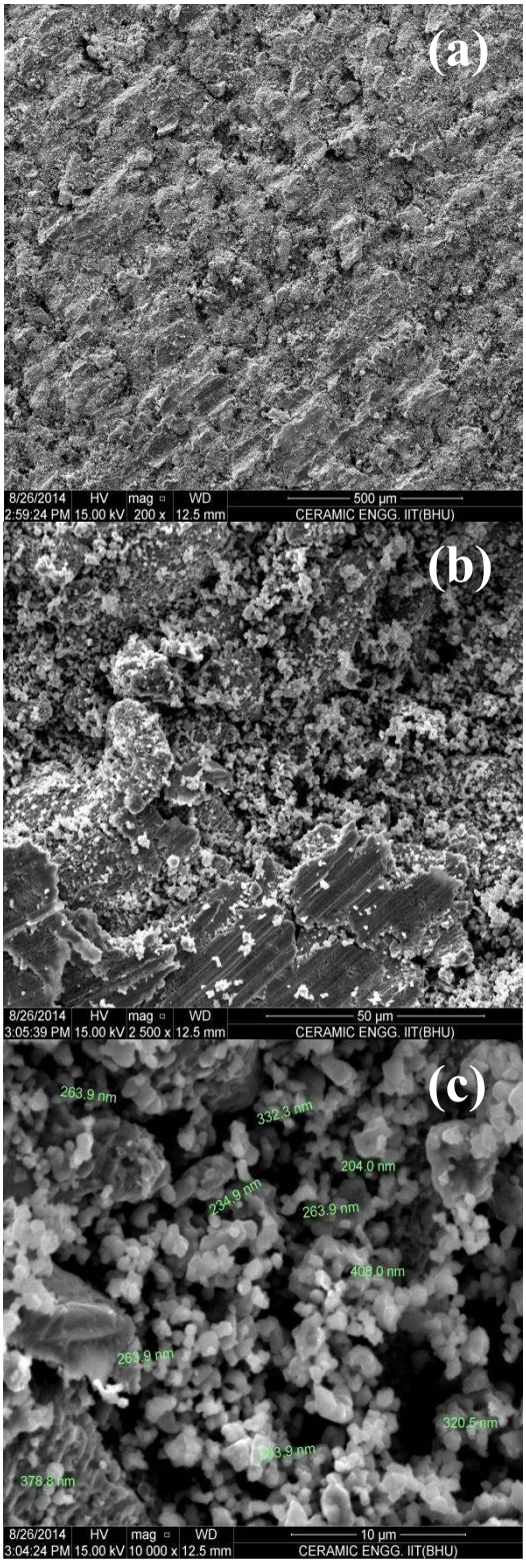

Fig. 7.21 SEM of worn specimen 10AFe1.0Ce1100(1) after wear test (a) 200X (b) 2500X and (c) 10000X

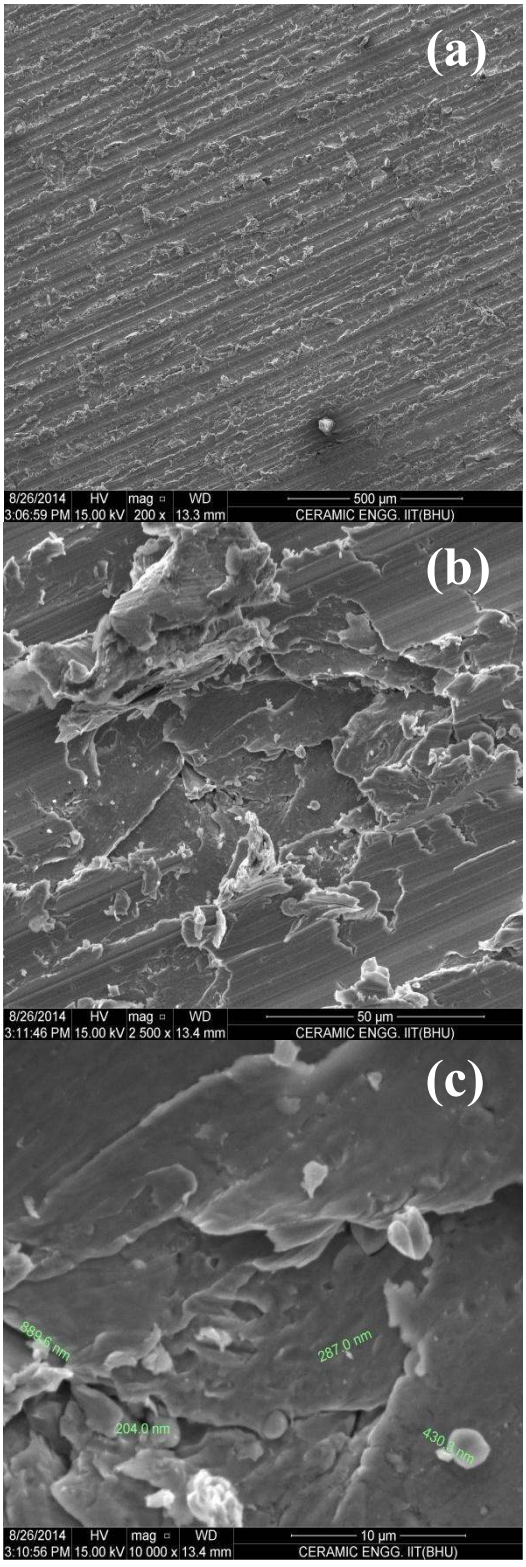

Fig. 7.22 SEM of specimen Pure Iron doped with 0.5% CeO_2 after wear test (a) 200X (b) 2500X and (c) 10000X

Fig. 7.20(a) shows the SEM image of specimen 10AFe0.5Ce1100(1) at 200X which shows the removal of the material due to the tangential skiving of the iron aluminate phase from the specimen surface. The removed debris material generates peel off marks on the specimen surface. Fig. 7.20(b) shows the SEM image of the same specimen at 2500X which clearly illustrates the adhesive wear as well as the micro-fracturing effect on the specimen surface. Due to the adhesive wear some polishing marks can be seen on the specimen surface whereas due to the micro-fracturing effect there is a removal of the material. The micro-fracturing effect can be attributed due to the presence of the hard cerium oxide particles. Fig. 7.20(c) shows the SEM image of the same specimen at 10000X which shows the nano size particles of iron aluminate phase. It also shows a strong bonding between the various nano size particles.

Fig. 7.21 shows SEM images of specimen 10AFe1.0Ce1100(1) after wear test (a) 200X (b) 2500X and (c) 10000X. Fig. 7.21(a) shows the SEM image of specimen 10AFe1.0Ce1100(1) at 200X which shows the removal of the material due to the tangential as well as due to the longitudinal skiving of the iron aluminate phase on the specimen surface. The removed debris material generates peel off marks on the specimen surface. Fig. 7.21(b) shows the SEM image of the same specimen at 2500X which clearly illustrates the adhesive wear as well as the abrasive wear effect on the specimen surface. Due to the adhesive wear some polishing marks can be seen on the specimen surface whereas due to the abrasive wear there is a removal of the material in the form of nano size particles. The abrasive wear effect can be attributed to the presence of hard iron aluminate and cerium oxide particles. Fig. 7.21(c) shows the SEM image of the same specimen at 10000X which shows the nano size particles of iron aluminate phase. It also shows a strong bonding between the various nano size particles. It is also interesting to note that since the hardness number of this particular specimen was high, therefore, the overall wear rate was also low amongst all the synthesized specimens.

Fig. 7.22 shows SEM images of specimen, pure iron doped with 0.5% CeO_2after wear test (a) 200X (b) 2,500X and (c) 10,000X. Fig. 7.22(a) shows the SEM image of the

specimen at 200X which illustrates the removal of the material due to the bilateral skiving of the iron aluminate phase on the specimen surface. Due to this bilateral skiving there is a generation of the grooves on the specimen surface. Fig. 7.22(b) shows the SEM image of the same specimen at 2500X which clearly illustrates the adhesive wear as well as layering of eroded material on the specimen surface. Fig. 7.22(c) shows the SEM image of the same specimen at 10000X which shows the micron and sub micron size particles of iron. It also shows a strong bonding between the various iron particles.

The present chapter discussed the effect of CoO and CeO_2 doping on Fe-Al_2O_3 metal matrix nanocomposites synthesized via powder metallurgy technique. In the current chapter it was also observed that how the small amount of doping can change the structural and mechanical behavior of the formed nanocomposites. It has been observed that on increasing the cobalt oxide percentage from 0.5 to 1.0% there was a significant reduction in the iron aluminate ($FeAl_2O_4$) phase formation. Microscopic images showed the nano size particles of Fe and Al_2O_3 separately. It was found in the present case that CoO particles bonds in between the particles of Fe and Al_2O_3 thereby reducing the reactive sintering rates. In the similar manner on increasing the cerium oxide percentage from 0.5 to 1.0% in the nanocomposite specimen there was formation of iron aluminate ($FeAl_2O_4$) phase along with the presence of separate cerium oxide phase. The hardness values were found to increase with an increase in the percentage of cerium oxide. Wear rate was found to decrease with the increase in the percentage of cerium oxide. It can be concluded that the various structural and mechanical properties were found to improve by doping CoO and CeO_2 in Fe-Al_2O_3 metal matrix nanocomposites.

The next chapter gives a detailed study on the structural and mechanical behavior of Fe-Al_2O_3-ZrO_2 hybrid metal matrix nanocomposite synthesized via powder metallurgy technique. Various properties investigated include phase, microstructure, density, hardness and wear respectively.